ACS APPLIED MATERIALS & INTERFACES

Research Article

www.acsami.org

Sensitive Detection of ssDNA Using an LRET-Based Upconverting Nanohybrid Material

Joe Gerald Jesu Raj,[†,‡] Marta Quintanilla,[‡] Khaled A. Mahmoud,[§] Andy Ng,[†] Fiorenzo Vetrone,[*,‡,¶] and Mohammed Zourob[*,†,⊥]

[†]Biosensors, Bio-MEMS, Bionanotechnology Laboratory (BBBL), Institute for Global Food Security, School of Biological Sciences, Queen's University, Queen's University Belfast, 18-30 Malone Road, Belfast, BT9 5BN, United Kingdom

[‡]Advanced Materials Laboratory, Institut National de la Recherche Scientifique - Énergie, Matériaux et Télécommunications, Université du Québec, Varennes, J3X 1S2 Québec, Canada

[§]Qatar Environment and Energy Research Institute, Qatar Foundation, Doha, Qatar

[⊥]Department of Chemistry, Alfaisal University, Al Zahrawi Street, Al Maather, Al Takhassusi Rd, Riyadh 11533, Saudi Arabia

[¶]Centre for Self-Assembled Chemical Structures, McGill University, 845 Sherbrooke Street West, Montreal H3A 0G4 Québec, Canada

Supporting Information

ABSTRACT: Water-dispersible, optical hybrid nanoparticles are preferred materials for DNA biosensing due to their biocompatibility. Upconverting nanoparticles are highly desirable optical probes in sensors and bioimaging owing to their sharp emission intensity in the visible region. We herein report a highly sensitive ss-DNA detection based on an energy transfer system that uses a nanohybrid material synthesized by doping $NaYF_4$:Tm^{3+}/Yb^{3+} upconverting nanoparticles (UCNPs) on silica coated polystyrene-*co*-acrylic acid (PSA) nanoparticles (PSA/SiO_2) as the donor, and gold nanoparticles (AuNPs) decorated with Ir(III) complex as the acceptor. UCNPs tagged on PSA/SiO_2 and the cyclometalated Ir(III)/AuNP conjugates were then linked through the ss-DNA sequence. Sequential addition of the target DNA to the probe molecular beacon complex resulted in the separation of the optical nanohybrid material and the quencher, leading to a measurable increase in the blue fluorescence emission intensity. Our results have shown a linear relationship between the fluorescence intensity and target DNA concentration down to the picomolar.

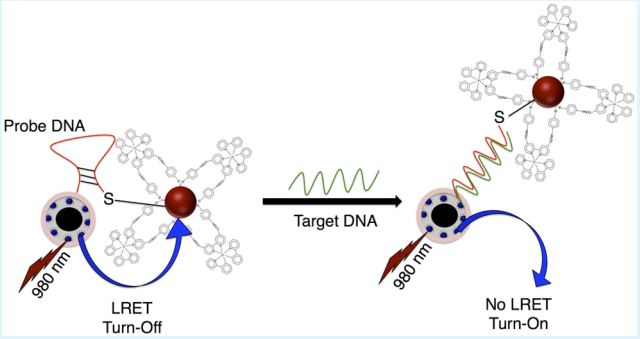

KEYWORDS: *nanohybrid, energy transfer, upconversion, biosensing, luminescence*

1. INTRODUCTION

Advancements in pharmacogenomics research, drug discovery, genetics, and infectious diseases, as well as the rapid development in DNA research, fuel the need to find more efficient fluorescent labels with improved characteristics. A wide range of fluorescent quantum dots (QDs) have been developed and successfully applied in biological analyses[1] and in FRET-based optical detection.[2] However, the use of QDs for detection of biomolecules has certain limitations due to their potential toxicity and high background signal in the presence of interfering fluorescent biomolecules. This problem is common with many other luminescent labels, such as organic dyes, since to get an efficient luminescent signal, they have to be excited in the ultraviolet or visible region of the electromagnetic spectrum.[3] A strategy to minimize the background signal is to move the excitation wavelength to the near-infrared (NIR) region. In this range, most organic molecules, as well as water, are transparent, thereby increasing the contrast of the luminescent signal since the excitation wavelength is specific to the optical probe. Recently, nanoparticles (NPs) doped with lanthanide ions (most commonly, Er^{3+}, Tm^{3+}, Yb^{3+}, and Ho^{3+}) have gained attention as functional nanomaterials for a variety of biological applications due to their sharp f−f emission peaks and long photoluminescence (PL) lifetimes.[4−6] In particular, when added as dopants to transparent host crystals, they provide the possibility of having UV, visible, and even NIR emissions after NIR excitation. This light transformation, known as upconversion (UC), is related to the presence of energy states energetically distributed in a way that several NIR photons can be sequentially absorbed to be emitted in one single step in the form of one higher-energy photon. Since those intermediate states are real electronic states of the ions, this excitation scheme can be carried out using low-cost, continuous-wave NIR diode lasers. Furthermore, the lanthanide

Received: April 8, 2015
Accepted: June 29, 2015
Published: August 17, 2015

DOI: 10.1021/acsami.5b02986
ACS Appl. Mater. Interfaces 2015, 7, 18257−18265

ions are inherently resistant to blinking, photobleaching, and photochemical degradation, which gives them an additional advantage over organic dye markers and QDs for biolabeling and bioassays.[7] For luminescence resonance energy transfer (LRET)-based sensors, the use of upconverting nanoparticles (UCNPs) also guarantees that donor and acceptor will not be excited at the same wavelength since the excitation of the UCNPs takes place at 980 nm NIR wavelength and hence reduces the possibility of autofluorescence and background interference. This also eliminates the disadvantage of spectral cross-talk signals or other possible errors during the measurement. For this reason, several LRET-based biosensors using UCNPs have been proposed recently, using different strategies and quenchers such as dyes, carbon dots, or gold nanoparticles.[8−13] As excellent luminescent quenchers, AuNPs open new perspectives to detect biomolecules with high sensitivity in FRET systems due to their high extinction coefficients as well as broad absorption spectrum within the visible light range that overlaps with the emission wavelengths of common energy donors.[14−17] Hairpin-shaped molecular beacons labeled with gold nanoparticles for DNA biosensing through fluorescence resonance energy transfer (FRET) have also been studied.[18] Up to single base DNA mismatch detection was successfully undertaken through the formation of a self-assembled nanostructure that uses gold nanoparticles and a fluorophore through conformational change mechanism.[19] UCNPs−AuNPs donor−acceptor pairs have attracted increasing attention as nanobiosensors for rapid and sensitive detection of virus.[20] Until recently, only bare AuNPs have been used as quenchers in the green spectral range since they show a strong absorbance related to the size-dependent plasmon resonance of the material around the 520 nm region. This limits the use of that donor−acceptor pair to the use of Er^{3+} ions as emitters due to their strong luminescence at green wavelengths, but the working range of UCNPs in LRET can be extended to different colors, which would provide the possibility of simultaneously using different sensing channels. The system proposed in this work uses UCNPs based on Tm^{3+} as the activator ion, which is advantageous owing to its upconverted blue emission, a possibility that has not been explored in detail for LRET sensing. For this purpose, a more effective AuNP that would absorb most of the donor emissions to enhance the sensitivity of the detection had to be developed. Cyclometalated iridium complexes have attracted significant interest due to their strong electrochemiluminescent property. Recently, a water-soluble Ir(III) complex with sugar appended ligands for the determination of antibiotics has also been reported.[21] Turn-on FRET-based luminescent Ir(III) probes have also been developed for the detection of cysteine and homocystein,[22] and very recently Li and co-workers have developed a DNA biosensor based on Ir(III) and applied successfully for cancer cell detection.[23] The iridium complex offers many advantages such as high stability in the solution state, high photoluminescence, and water solubility, which makes it suitable for bioanalysis. In the present work, we have developed a highly sensitive biosensor for the detection of target DNA sequence using $NaYF_4$:Tm^{3+}, Yb^{3+} UCNPs on PSA/SiO_2 nanohybrids as donors and iridium-bipyridyl complex immobilized on AuNPs as quenchers. Additionally, to the best of our knowledge there has been no report on the use of UCNPs as an optical biosensor in conjugation with a cyclometalated Ir(III)-AuNP complex as quencher for the detection of ssDNA.

2. EXPERIMENTAL SECTION

2.1. Chemicals. Styrene (St) and acrylic acid (AA) were purchased from Aldrich and distilled under reduced pressure. Potassium persulfate (KPS) was recrystallized from deionized water prior to use. Aqueous ammonia solution ($NH_3·H_2O$, 28%), 4-aminobenzenethiol (4-ABT > 98%), tetraethoxysilane (TEOS > 98%), anhydrous ethanol, and 3-aminopropyltriethoxysilane (APTES), (3-glycidyloxypropyl)trimethoxysilane (GPTMS), and chloroauric acid tetrahydrate ($HAuCl_4·H_2O$), 2-phenylpyridine, $IrCl_3·3H_2O$, 2-ethoxyethanol, 2,2′-bipyridine-4,4′-dicarboxylic acid, sodium acetate, ammonium hexafluorophosphate, trisodium citrate were purchased from Aldrich. Y_2O_3, Yb_2O_3, Tm_2O_3, trifluoracetic acid, sodiumtrifluoroacetate, oleic acid, octadecene, and citric acid were obtained from Alfa Aesar. Triton X-100 (TX-100), *n*-hexanol, methanol, hexane, toluene, ethanol, dichloromethane, acetone, anhydrous *N*,*N*-dimethylformamide (DMF), ammonia solution (25%, w/w), 1-ethyl-3-(3-(dimethylamino)propyl) carbodiimide hydrochloride (EDC), *N*-hydroxysulfosuccinimide (sulfo-NHS), and succinic anhydride (>97%) were purchased from Fluka (USA). Highly pure water (Millipore) of resistivity greater than 18.0 MΩ cm was used in all experiments. All chemicals were used as received unless specified.

All chemicals were used as received unless specified. DNA oligonucleotides with a concentration of 100 nM were purchased from Integrated DNA Technologies (IDT), and the sequences are listed as follows (the stem DNA sequences have been underlined; single base mismatch is *italicized*): Sequence Description: B1-NH_2-thiol. Sequence: 5′-/5AmMC6/GC GAG AAG TTA AGA CCT ATG CTC GC/3ThioMC3-D/-3′. Complementary: 5′-CAT AGG TCT TAA CTT-3′. Single base mismatch: 5′-CAT AG*T* TCT TAA CTT-3′. Negative control: 5′-AAA AAA AAA AAA AAA-3′.

2.2. Instrumentation. FTIR was recorded on a Thermoscientific Nicolet Spectrometer using FTIR grade KBr as background. TEM images were obtained with a Philips CM200 High-Resolution TEM (HRTEM). The morphology and size distribution of the UC, gold, and polymer nanoparticles were observed on carbon coated copper grid. Prior to analysis, a 10 mg UCNP sample was dispersed in 10 g of hexane and sonicated for 1 h. A drop of the resulting solution was evaporated on a Formvar/carbon film supported on a 300 mesh copper grid (3 mm in diameter). For the PSA, PSA/SiO_2, and UCNP tagged PSA/SiO_2 nanoparticles, respective ethanolic solutions have been dropped on the TEM grid.

^{1}H NMR spectra were recorded on a Bruker 400 MHz instrument using $CDCl_3$ solvent. ^{13}C NMR spectra were recorded on a Varian S-500 instrument at 125 MHz using deuterated acetone solvent. XPS was recorded on a VG Escalab 220i XL instrument equipped with 6 channeltrons using unmonochromated Mg K X-ray source (1253.6 eV). The phase identification was done from the X-ray diffraction (XRD) patterns recorded using a Bruker D8 Advance Diffractometer for powder samples with Cu KR radiation at λ = 0.154 nm operating at 45 kV and 40 mA.

The upconversion emission spectra were obtained using a Thorlabs fiber-coupled 975 nm laser diode (maximum power of 330 mW) as the excitation source. For the OA capped hydrophobic UCNPs the sample (1 wt % in hexane) were placed in 10 mm path-length quartz cuvettes (Hellma, QS). For PSA, PSA/SiO_2, and UCNP doped PSA/SiO_2 nanoparticles, DNA tagged UCNP doped nanohybrids, their ethanol solutions were used. The emission light was collected by a lens in a 90° configuration, and then transferred to a spectrophotometer (Avaspec-2048L-USB2) using an optical fiber. All along the experiments, the cuvette had been placed in a fixed sample holder that guarantees a comparable laser focalization over the sample for every sample, and thus, the possibility to compare intensities between different samples. To check that, every spectrum has been recorded removing and placing again the same sample, demonstrating an experimental error generally lower than 5%.

2.3. Synthesis of Precursor Complex [(ppy)$_2$Ir(μ-Cl)]$_2$. The iridium complex was synthesized according to the literature procedure with a slight modification.[24] Briefly, a mixture of 2-phenylpyridine (0.34 g, 2.2 mmol), $IrCl_3·3H_2O$ (0.34 g, 1 mmol) in a mixed solvent of

DOI: 10.1021/acsami.5b02986
ACS Appl. Mater. Interfaces 2015, 7, 18257−18265

2-ethoxyethanol (15 mL) and water (5 mL) was stirred under N_2 at 120 °C for 20 h. The precipitate was then cooled to room temperature and collected by filtration and washed with water, ethanol, and acetone, respectively, and subsequently dried in vacuum to give the $[(ppy)_2Ir(\mu\text{-}Cl)]_2$ dimer complex.

^{1}H NMR (500 MHz, $CDCl_3$) δ: 9.26 (d, J = 5.5 Hz, 1H), 7.96 (d, J = 8 Hz, 1H), 7.82 (t, J = 7.5 Hz, 1H), 7.58 (d, J = 7.5 Hz, 1H), 6.85 (m, 2H), 6.63 (t, J = 7.5 Hz, 1H), 5.89 (d, J = 8 Hz, 1H). ^{13}C NMR (125 MHz, acetone-d_6) δ: 168.2, 151.8, 143.5, 144.1, 135.7, 132.4, 129.7, 126.8, 121.8, 121.6, 119.8 ppm. Calcd for $C_{44}H_{32}Cl_2Ir_2N_4$: C, 49.29; H, 3.01; N, 5.23. Found: C, 49.32; H, 3.07; N, 5.24. ESI-MS: 1072 [M^+].

2.4. Synthesis of $[(ppy)_2Ir(dcbpy)]^+$ PF_6^-. $[(ppy)_2Ir\ (\mu\text{-}Cl)]_2$ (0.21 g, 0.2 mmol) was prepared as a solution in dichloromethane (15 mL) and added to a suspension of 2,2′-bipyridine-4,4′-dicarboxylic acid (0.098 g, 0.4 mmol) in methanol (20 mL). The reaction mixture was then heated to reflux with stirring for 4 h. To this solution, sodium acetate (excess) in methanol (5 mL) was added, and the mixture was stirred for a further 45 min. The solvent was then removed under reduced pressure, hydrochloric acid (1 M, 10 mL) was added, and the suspension was stirred for 20 min. The product was then filtered, washed with water (2 × 25 mL), and vacuum-dried, and the solid was then dissolved in methanol. A saturated solution of ammonium hexafluorophosphate in methanol (5 mL) was then added, and the mixture was stirred for a further 45 min. The solvent was removed under reduced pressure, and the residue was extracted into dichloromethane and filtered. The solvent was removed under reduced pressure to yield $[(ppy)_2Ir(dcbpy)]^+$ PF_6^- as a dark-red powder. The crude product was flash chromatographed on silica gel using CH_2Cl_2 as an eluent to afford the desired Ir(III) complex. (0.16 g, 69%).

^{1}H NMR (500 MHz, $CDCl_3$) δ: 6.32 (d, J = 5.9 Hz, 2H), 6.24 (t, J = 7.22 Hz, 2H), 6.54 (m, 2H), 6.64 (t, J = 7.46 Hz, 2H), 7.22 (t, J = 7.34 Hz, 2H), 7.52 (d, J = 7.50 Hz, 2H), 7.48 (t, J = 7.50 Hz, 2H), 7.58 (t, J = 7.56 Hz, 2H), 7.83 (m, 2H), 8.46 (d, J = 5.52 Hz, 2H), 9.38 (s, 2 H). ^{13}C NMR (125 MHz, acetone-d_6) δ: 121.08, 123.85, 124.77, 125.77, 126.07, 129.29, 131.53, 132.6, 139.91, 142.41, 145.05, 150.59, 150.82, 152.83, 157.77, 165.56, 168.65 ppm. mp (°C): 194.5 Calcd for $C_{34}H_{24}F_6N_4O_4IrP$: C, 45.87; H, 2.69; N, 6.31. Found: C, 46.13; H, 2.84; N, 6.74. IR (KBr): ν 2934 (s, OH), 1726 (s, CO), 852 (s, PF) cm^{-1}. ESI-MS: 745 [M^+].

2.5. Synthesis of Activated $[(ppy)_2Ir(dcbpy)]$-Sulfo-NHS Ester. EDC (0.17g, 1.11 mmol) and Sulfo-NHS (0.119 g, 1.035 mmol) were dissolved in acetonitrile (2 mL) with stirring and cooled in an ice bath. The $[(ppy)_2Ir(dcbpy)]^+PF_6^-$ solution in acetonitrile (100 μL, 4.3 × 10^{-4} M) was added to the EDC-NHS mixture. The solution was stirred for 3 h at room temperature to form the $[(ppy)_2Ir(dcbpy)]$-sulfo-NHS ester. This ester (2.69 × 10^{-5} M) was kept at 4 °C for further use.

2.6. Synthesis of AuNPs. Prior to the synthesis of AuNPs, all glassware used was cleaned in a bath of freshly prepared 3:1 $HCl:HNO_3$ and rinsed thoroughly with water before using. Typically, 99 mL triple-distilled water and 1 mL 1% $HAuCl_4$ solution were added into a round-bottom flask equipped with a reflux condenser under vigorous stirring. The flask was subsequently incubated in an oil bath to reflux under stirring. Under the boiling solution, 5 mL of 1% trisodium citrate solution was quickly added to the flask, and the reaction was allowed to reflux for another 20 min. The color of the solution changed from pale yellow to deep red and the solution was cooled to room temperature and then stored at 4 °C in the refrigerator for further use. The average diameter of the synthesized gold nanoparticle was 24 nm.

2.7. Attachment of Activated $[(ppy)_2Ir(dcbpy)]$-NHS Ester to Gold Nanoparticles to Form Ir(III)-Gold Nanoparticle Conjugates. One mole of the $(ppy)_2Ir(dcbpy)]$-NHS ester was added to a 2 mol ethanol solution of 4-ABT and the mixture was stirred at room temperature for 2 h resulting in the formation of $[(ppy)_2Ir(dcbpy)(4\text{-}ABT)_2]$. To this mixture, 1 mL of the gold colloid was added and the mixture was stirred for another 2 h for the attachment of the −SH functional group from the 4-ABT linker molecule in the iridium complex onto the surface of AuNPs. The resultant solution was then centrifuged and the supernatant was removed. The precipitate containing Ir(III)-AuNP conjugates was then washed several times with ethanol and finally dispersed in water for further use. ^{1}H NMR (500 MHz, $(CD_3)_2SO$ δ: 6.6−7.2 (m, Ar-*H*), 2.2 (RCON*H*), 3.2−3.8 (b, Au−S).

2.8. Synthesis of Poly(styrene-*co*-acrylic acid) (PSA) Nanoparticles. PSA nanoparticles were prepared according to the method described here. 1.6 g of styrene, 0.4 g of acrylic acid (AA), and 100 mL of H_2O were added into a three-necked flask, which was equipped with a mechanical stirrer and a condenser. The solution was purged with nitrogen to remove oxygen for 30 min and then heated to 80 °C. Subsequently, 0.06 g of KPS dissolved in 2 mL of H_2O was injected into the reaction mixture to initiate the polymerization under stirring and this reaction system continued heating for 10 h. The resulting PSA nanoparticles were washed with ultrapure water by centrifugation several times and then dispersed in water for further use.

2.9. Synthesis of PSA/SiO_2 Nanostructures. The as-prepared PSA nanoparticles were encapsulated in silica. Typically, PSA nanoparticles were dispersed in a mixture of 9 mL of water, 40 mL of ethanol, and 1 mL of ammonia solution by sonication for 20 min. TEOS was added to the mixture, and the sonication was continued at 0 °C for another 2 h. The obtained products were washed repeatedly with ethanol and water to eliminate excess TEOS. Finally, the sample was dispersed in water for further use.

2.10. Synthesis of Oleate-Capped $NaYF_4$:Tm^{3+}, Yb^{3+} Co-doped Upconverting Nanoparticles (UCNPs). ***Caution:*** *This high temperature reaction involves liberation of very toxic and corrosive fluoro compounds, hence proper care must be taken and the reaction must be carried out in a well-ventilated fume hood.* $NaYF_4$:Tm^{3+}, Yb^{3+} UCNPs were synthesized via the thermal decomposition method reported earlier.[25] Briefly, the metal (Y^{3+}, Tm^{3+}, and Yb^{3+}) trifluoroacetates (prepared by reacting Y_2O_3 (1 mmol), Yb_2O_3 (0.27 mmol), and Tm_2O_3 (0.005 mmol), and refluxing the corresponding oxides in 50/50 v/v CF_3COOH/H_2O at 80 °C) were mixed with CF_3COONa (2.5 mmol), oleic acid (20 mL), and 1-octadecene (20 mL). The resulting mixture was heated to 110 °C with constant stirring under vacuum. After 30 min, the temperature of the mixture was increased to 330 °C at a rate of 5 °C per minute under Ar flow. At this final temperature, the mixture remained for 1 h, after which it was allowed to cool to 70 °C prior to precipitation with absolute ethanol. The nanocrystals were then separated via centrifugation and further purified by dispersing in hexane followed by precipitation with ethanol.

2.11. Synthesis of Hydrophilic $NaYF_4$:Tm^{3+}, Yb^{3+} UCNPs. The as-synthesized oleate-capped hydrophobic UCNPs were made water dispersible by a ligand exchange method. Briefly, 0.1 g of citric acid was mixed with 10 mL of ethanol. To this, 5 mL of chloroform containing 0.05 g of the oleate-capped UCNPs was added. The mixture was sonicated for 1 h and left stirring overnight at room temperature. The solution was then centrifuged at 8000 rpm for 1 h and the pellet was washed several times with ethanol and water. Finally, the citrate-capped UCNPs were dispersed in water for further use.

2.12. Synthesis of $NaYF_4$:Tm^{3+}, Yb^{3+} Decorated PSA/SiO_2 Nanohybrids. 1 mL of Tm^{3+}, Yb^{3+} codoped hydrophilic $NaYF_4$ UCNPs was added to 1 mL of PSA/SiO_2 nanohybrids in a centrifuge tube. The mixture was incubated at room temperature overnight. To this resultant sample solution, 10 mL of dry ethanol was added and the mixture was sonicated for 1 h. The solution was then centrifuged at 8000 rpm for 20 min and the supernatant was removed. The precipitate containing the $NaYF_4$:Tm^{3+}, Yb^{3+} decorated PSA/SiO_2 nanohybrids was washed with water and dispersed in ethanol.

2.13. Surface Modification $NaYF_4$:Tm^{3+}, Yb^{3+} Decorated PSA/SiO_2 Nanohybrids with Epoxy Groups. GPTMS is a silane-coupling agent and can covalently bind to the surface of silica spheres by condensation of the methoxysilane groups (Si−O−CH_3) and silanol groups (Si−OH) of the silica surfaces. To accomplish this, 15 mg of the $NaYF_4$:Tm^{3+}, Yb^{3+} decorated PSA/SiO_2 nanohybrids were dispersed in 70 mL of ethanol through sonication, and then a 0.1 mL of GPTMS was added to the mixture during magnetic stirring. After the reaction mixture was refluxed for 5 h at 120 °C, the resulting

DOI: 10.1021/acsami.5b02986
ACS Appl. Mater. Interfaces 2015, 7, 18257−18265

product was centrifuged several times with ethanol to remove excess reactants and redispersed in ethanol.

2.14. Conjugation of Epoxy Modified $NaYF_4$:Tm^{3+}, Yb^{3+} Decorated PSA/SiO_2 Nanohybrids with Probe Oligonucleotides. 2 mg of the $NaYF_4$:Tm^{3+}, Yb^{3+} decorated epoxy modified PSA/SiO_2 nanohybrids was dispersed in 5.0 mL of 0.1 mol L^{-1} phosphate buffer (pH 7.0) by ultrasonication and a homogeneous dispersion was obtained. An amount of 25 mg of succinic anhydride was added to the solution, and then the mixture solution was allowed to react for 2 h under stirring. After reaction, the as-prepared mixture solution was centrifuged and washed with phosphate buffer (pH 7.0), and then redispersed in 5.0 mL of 0.05 M Tris-HCl buffer containing 0.02 M NaCl (pH 7.2). 1.2 mg of EDC and 1.8 mg of NHS were added to the solution and the reaction was allowed to react for 30 min under stirring. 50 μL of ssDNA was then added, and the reaction was incubated for 12 h. The resulting solution was centrifuged and washed with 0.05 M Tris-HCl, the particles were resuspended in 5.0 mL of 0.05 M Tris-HCl buffer containing 0.02 M NaCl (pH 7.2), and therefore the PSA/SiO_2 conjugated with oligonucleotide; PSA/SiO_2NPs//ssDNA-Probe was obtained.

2.15. Conjugation of Ir(III)-AuNPs Conjugates with UCNP-Decorated PSA/SiO_2NPs//ssDNA-Probe. The conjugation of Ir(III)-AuNPs with the oligonucleotide was accomplished according to the following procedure. 1.0 mL of the as-prepared Ir(III)-AuNPs was transferred into a microcentrifugation tube and centrifuged for 15 min. The nanohybrids were resuspended in 1.0 mL of 10 mM phosphate buffer (pH 7.0). Twenty milliliters of the $NaYF_4$:Tm^{3+}, Yb^{3+} decorated PSA/SiO_2NPs//ssDNA-Probe was added to the 1.0 mL of Ir(III)-AuNPs dispersion, and the mixture was allowed to react for 16 h at 50 °C. Then, saline phosphate buffer (10 mM phosphate buffer containing 2 M NaCl, pH 7.0) was added dropwise to the solution to reach a final salt concentration of 0.1 M NaCl, and then the reaction continued for 40 h. The solution was centrifuged and resuspended several times. After centrifuging, the nanohybrids were dispersed in 10 mM phosphate buffer containing 0.1 M NaCl (pH 7.0), and thus PSA/SiO_2 NPs//ssDNA(Probe)//Ir(III)-AuNP were obtained.

2.16. DNA Hybridization Assay for LRET Measurements. For the FRET measurements, sample solutions containing 0.05 mg/mL of the PSA/SiO_2 NPs//ssDNA(Probe)//Ir(III)-AuNP in phosphate buffer were incubated with different concentrations of target ssDNA sequences at 35 °C for 1 h. Then, LRET upconversion measurements were done on all these solutions at 975 nm excitation.

3. RESULTS AND DISCUSSION

The proposed UCNP-LRET biosensor is based on the quenching of the visible emissions produced by $NaYF_4$:Tm^{3+}, Yb^{3+} UCNPs following excitation with 975 nm light. The efficiency of this quenching, as usually happens in LRET processes, will be dependent on the distance between the donor (UCNPs), and the $[(ppy)_2Ir(dcbpy)]^+PF_6^-$−AuNP conjugates as energy acceptors. When immobilized on the surface of AuNPs, the cyclometalated Ir(III) complexes showed a broad absorption from 300 to 800 nm, making $[(ppy)_2Ir(dcbpy)]^+PF_6^-$/AuNP conjugates excellent quenchers for LRET-based optical detection. LRET biosensor based on UCNPs offers an additional advantage: instead of directly quenching the probe signal, in this case the blue emission, it would affect the base of the upconverting process, thus reinforcing the separation between light coming from the donor and possible emissions coming from the acceptor. The presence of a large number of conjugated double bonds in the cyclic aromatic ligands in the iridium complex on the surface of the gold nanoparticles promotes the multiphonon relaxation process at the intermediate levels in the upconversion mechanism and hence quenches more effectively the visible emission of the donor upconversion nanoparticles. For the donor nanostructures, PSA nanoparticles were synthesized from their corresponding monomers. TEM (Figure 1) shows monodispersed spheres with an average size of 300 nm.

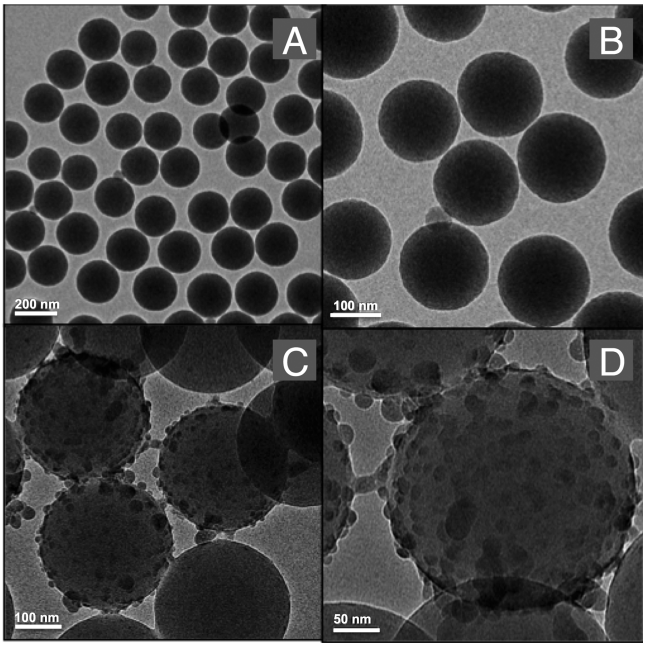

Figure 1. TEM images of (A) as-synthesized polystyrene-*co*-acrylic acid (PSA) nanoparticles, (B) silica-coated PSA nanoparticles (PSA/SiO_2), (C) $NaYF_4$:Tm^{3+}/Yb^{3+} tagged PSA/SiO_2 nanoparticles, and (D) HRTEM of $NaYF_4$:Tm^{3+}/Yb^{3+} tagged PSA/SiO_2 nanoparticles.

Small-sized $NaYF_4$:Tm^{3+}, Yb^{3+} UCNPs were then synthesized through a thermal decomposition method.[25] The TEM image shows that the synthesized $NaYF_4$:Tm^{3+}, Yb^{3+} UCNPs were cubic in shape and the average diameter of the cubic-phase nanoparticles was approximately 20 nm. The XRD pattern of the UCNPs (Figure S3 Supporting Information) against the standard (JCPDS: 06−0342) confirmed the cubic phase of the nanoparticles and the positions of the peaks in the XRD with reference to the standard are in excellent correlation, thereby confirming the absence of any other phases or impurities. Intensity of the peaks on XRD confirmed the highly crystalline nature of the as-synthesized upconversion nanoparticles. To confirm the particle size, TEM measurements were carried out and the average crystallite size of the UCNPs was calculated according to Scherrer's equation. $D = K\lambda/\beta \cos\theta$; where $K = 0.89$, D is the crystallite size (in nm), λ is the wavelength of Cu Kα radiation, β is the corrected half-width of the diffraction peak, and θ is the Bragg's diffraction peak angle.

According to this equation, the average crystallite size of the UCNPs was found to be 20 nm, which is in excellent agreement with the TEM results. The hydrophobic oleate-capped UCNPs were rendered hydrophilic through a ligand exchange procedure using the hydrophilic citrate ligand. Subsequently, the hydrophilic UCNPs were then incubated with PSA/SiO_2 nanostructure to form the nanohybrid PSA/SiO_2/UCNPs material (Figure 1C,D). The surface of the composite material was then grafted with (3-glycidyloxypropyl)trimethoxysilane (GPTMS) in order to endow it with epoxy functional groups for ssDNA conjugation through nucleophilic addition. The surface functionalization of this composite material has also been confirmed using FTIR spectroscopy (Figure 2). The

DOI: 10.1021/acsami.5b02986
ACS Appl. Mater. Interfaces 2015, 7, 18257−18265

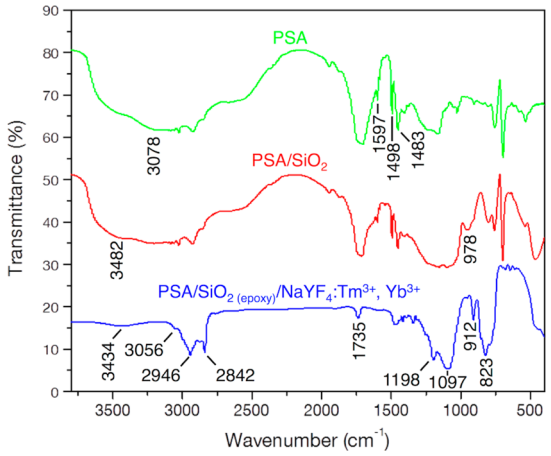

Figure 2. FTIR spectra of PSA nanoparticles, PSA/SiO_2 and PSA/$SiO_{2\ (epoxy)}$/$NaYF_4$: Tm^{3+}, Yb^{3+}.

analysis of the parent PSA nanoparticles was performed and various peaks were observed. Specifically, the peak at 3078 cm^{-1} was attributed to the aromatic CH stretching vibration, while the intense sharp peaks at 1483, 1498, and 1597 cm^{-1} were ascribed to the aromatic C−C stretching frequencies. Following the growth of silica, these intensities were observed to be considerably weaker for the PSA/SiO_2 nanoparticles. Moreover, peak broadening was observed between 1000 and 1250 cm^{-1} and was due to the extensive silica coating on the surface of PSA nanoparticles. The Si−OH stretching vibration has been confirmed by the peak at 978 cm^{-1}.

As stated previously, the hydrophobic $NaYF_4$:Tm^{3+}, Yb^{3+} UCNPs were rendered hydrophilic using the citrate ligand in order to assemble the hybrid structure. The final PSA/$SiO_{2(epoxy)}$/$NaYF_4$:Tm^{3+}, Yb^{3+} (citrate stabilized) structure was analyzed using FTIR spectroscopy and peaks at 2842 and 2946 cm^{-1} confirmed the CH stretching vibrations of the citrate-capped UCNPs present on the PSA/SiO_2 nanohybrids.

Two characteristic absorptions of the epoxide ring, owing to the subsequent GPTMS functionalization, were also observed. The first one at 912 cm^{-1} was attributed to the C−O deformation of the epoxide group, while the second band, located at 3056 cm^{-1}, was attributed to the C−H stretching of the methylene group of the epoxy ring. The peak at 1735 cm^{-1} was due to the carbonyl stretching vibration of the carboxyl group of citric acid and the peaks at 1097 and 1198 cm^{-1} were associated with the symmetrical and asymmetrical stretching vibrations, respectively, of the citric acid carboxylic functional groups bound to the surface of the UCNPs. The peak at 823 cm^{-1} was attributed to the Si−O−CH_3 stretching vibration from the GPTMS reagent for epoxy functionalization. In another synthesis the cyclometalated $[(ppy)_2Ir(dcbpy)]^+PF_6^-$ complex was prepared and functionalized on the surface of AuNPs using 4-aminobenzenethiol (4-ABT) as linker. These $[(ppy)_2Ir(dcbpy)]^+PF_6^-$−AuNP conjugates and the as-prepared PSA/SiO_2/UCNP hybrid structure were linked through the probe ssDNA sequence as described in the Experimental Section.

Upconversion in thulium ions is a third-order process[26] (at least, three excitation NIR photons are needed to emit one blue photon). Therefore, in order to have a good signal/noise ratio on the luminescence intensity, we increased the amount of UCNPs in the donor side of the sensor. The use of PSA/SiO_2/UCNPs nanohybrids was considered to be an attractive option due to their excellent optical properties, biocompatibility, as well as the available large surface area, which makes it possible for the development of real-time analysis of multiple analytes with multimodal optical probes. This nanohybrid also acts as a platform for biomolecular reaction to take place on its surface. We used $[(ppy)_2Ir(dcbpy)]^+PF_6^-$ anchored AuNPs as effective quenchers in the LRET-based optical detection since the iridium−metal complex on the surface of AuNPs offers good stability and biocompatibility. The presence of carboxyl functional groups on the $[(ppy)_2Ir(dcbpy)]^+PF_6^-$ complex makes it water-soluble and thus amenable to bioconjugation. The carboxyl functional groups of the $[(ppy)_2Ir(dcbpy)]^+PF_6^-$ complex was attached to the $-NH_2$ end of the 4-ABT using EDC-NHS conjugation chemistry and its −SH end was directly attached to the surface of the AuNPs. In order to synthesize the nanohybrid, AuNPs were first synthesized and subsequently attached to the 4-ABT thiol linker. Attachment of the Ir complex on the surface of AuNPs through the 4-ABT thiol linker molecule through EDC/NHS conjugation chemistry was confirmed by X-ray photoelectron spectroscopy (XPS) measurements (Figure S4 B). Investigation of XPS spectrum showed the presence of all the elements from the Ir complex at their respective binding energy values. The UV−vis absorption spectrum of the thiolated AuNPs showed a red shift with absorption maximum centered at 544 nm thus confirming the attachment of 4-ABT linker molecule and the Ir complex on the AuNP surface[27] (Figure S4 C). On the other side of the nanoparticle assembly the available epoxy functional groups on the surface of the UCNP decorated PSA/SiO_2 nanohybrids were attached to the amino end of the probe ssDNA sequence and its thiol end was connected to the $[(ppy)_2Ir(dcbpy)]^+PF_6^-$ modified AuNP leading to the formation of PSA/SiO_2/$NaYF_4$:Tm^{3+}, Yb^{3+}//ssDNA//$[(ppy)_2Ir(dcbpy)(4\text{-}ABT)_2]$/AuNP.

The synthesized AuNPs possess a plasmon resonance peak at 520 nm (Figure 3A, red solid line). When the AuNPs were decorated with $[(ppy)_2Ir(dcbpy)]^+PF_6^-$ complex, the plasmon resonance of the $[(ppy)_2Ir(dcbpy)]^+PF_6^-$-AuNP conjugates showed a red shift and the entire absorption spectrum extended from 500 to 800 nm with an absorption maximum appearing at

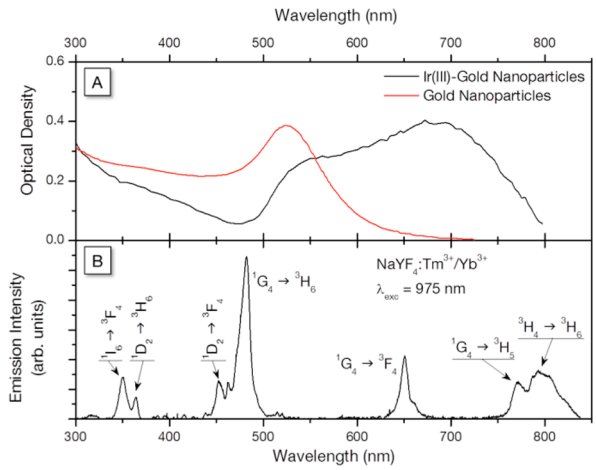

Figure 3. (A) UV−vis absorption spectrum of the AuNPs (red line) and iridium complex $[(ppy)_2Ir(dcbpy)(4\text{-}ABT)_2]$ immobilized on AuNPs (black line). (B) Upconversion emission spectrum of $NaYF_4$:Tm^{3+}, Yb^{3+} in hexane with corresponding energy level transitions following excitation with 975 nm.

DOI: 10.1021/acsami.5b02986
ACS Appl. Mater. Interfaces 2015, 7, 18257−18265

700 nm (Figure 3A). The various energy level transitions (Figure 3B) involved within the UCNPs overlap with the Ir(III) anchored AuNPs making it an excellent quenching material for LRET technique. The quenching of the visible emission from $NaYF_4$:Tm^{3+}, Yb^{3+} by the Ir(III)-AuNP conjugates has been possible via two different processes, such as radiative and nonradiative. In the radiative energy transfer (reabsorption), the photons emitted by the UCNPs at each wavelength will be absorbed by the quencher. Thus, this process takes place at every wavelength where the UCNPs are emitting (Figure 3B), and the Ir(III) decorated AuNPs are absorbing (Figure 3A). On the other hand, the nonradiative energy transfer is an exchange interaction that takes place faster than the emission of photons by the UCNPs. Consequently, it will take place when the UCNPs (donors) and the quencher (acceptor) transitions are characterized by the same energy.

It is evident that broadening of absorption of the quencher resulted from the surface functionalization of AuNPs by the Ir complex. The broadening of the absorption spectrum of the quencher is a favorable characteristic feature in two ways. First, from the radiative energy transfer point of view, more emissions are affected by the quencher. Second, from the nonradiative point of view, absorption of the Ir decorated AuNPs is now resonant both with $^3F_{2,3} \rightarrow {}^3H_6$ and $^1G_4 \rightarrow {}^3F_4$ transitions of the Tm^{3+} ions. As a result, such acceptors would likely interrupt the usual upconverting path, consequently quenching the visible emissions related to the higher-energy excited states. The principle of the LRET based nanosensor is shown in Scheme 1A,B. The scheme showed a hairpin-shaped molecular beacon with an UCNP-decorated PSA/SiO_2 nanohybrids as donor at one end and the [$(ppy)_2Ir(dcbpy)(4\text{-}ABT)_2$]/AuNPs conjugate as an acceptor at the other end. The presence of Ir(III) modified AuNPs quenches the emission intensity of UCNPs (turn-off) when excited at 975 nm (Scheme 1A). When the complementary DNA sequence is added to the complex, both nanoparticle assemblies moved further due to the formation of elongated hybridized double helical structure. In turn, the probability of luminescent energy transfer between them is reduced, thereby restoring the emission intensity (turn-on) of the donor UCNPs (Scheme 1B). To calibrate the sensitivity of the prepared complex, the luminescence emission of the samples with the same concentration of probe DNA complexes were titrated against different concentrations of target DNA down to 1 pM. The addition of negative control to the probe molecular beacon connected nanohybrids, PSA/SiO_2NPs/$NaYF_4$:Tm^{3+},Yb^{3+}//$ssDNA_{(Probe)}$//Ir(III)-AuNP showed almost no change in the upconversion emission intensity, thus confirming the sensitivity of our method (Figure 4D). To confirm the selectivity of our nanosensor, we titrated the probe DNA conjugated nanohybrids with single base mismatch. Measurement of upconversion emission proved that the blue emission still remained almost quenched (Figure 4D) upon excitation, thus confirming the highly selective nature of the proposed nanobiosensor.

The emission intensity (Figure 4A) is proportional to the concentration of target DNA sequence in the sample, as a consequence of hybridized elongated double helical DNA structure, which resulted in the increased distance between the [$(ppy)_2Ir(dcbpy)(4\text{-}ABT)_2$]/AuNP and the UCNP decorated PSA/SiO_2 nanohybrids. It is clear from the Figure 4A that the high signal/background contrast in the whole concentration range is considered, especially taking into account that no background or baseline has been removed from the spectrum.

Scheme 1. (A,B) Simplified Schematic Illustration of the Proposed LRET-Based Detection of ssDNA Using UCNP Decorated PSA/SiO_2 Nanohybrids and Cyclometalated Ir(III)-AuNPs.[a] (C) Plausible Luminescent Resonant Energy Transfer from UCNPs to Ir Decorated AuNPs

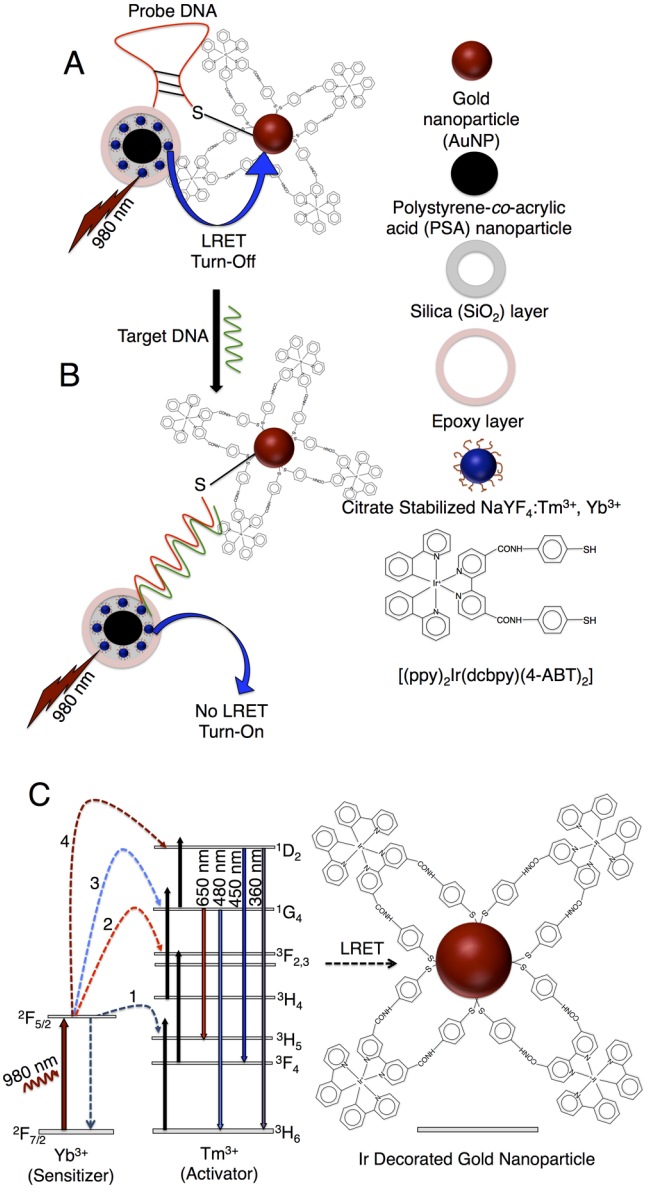

[a]It should be noted that only a single ssDNA is shown for simplicity.

This clearly demonstrates the reliability and simplicity of the proposed technique. For calibration purposes, the area under the emission bands (Figure 4A) has been plotted against the target DNA concentration (Figure 4B). From Figure 4B, it is evident that both magnitudes are related through a linear dependency in a semilogarithmic plot, which provides the sensitivity curve for the ssDNA nanobiosensor. The fact that the dependency between both magnitudes is not linear can be attributed to the nonlinear nature of upconversion processes. In particular, for Tm^{3+}, Yb^{3+} doped nanoparticles after 975 nm excitation, the upconversion mechanism necessary to emit blue light is at least a third-order process. In the proposed quenching strategy, the luminescence is being blocked from the NIR-emitting level that works as an intermediate step for the

DOI: 10.1021/acsami.5b02986
ACS Appl. Mater. Interfaces 2015, 7, 18257−18265

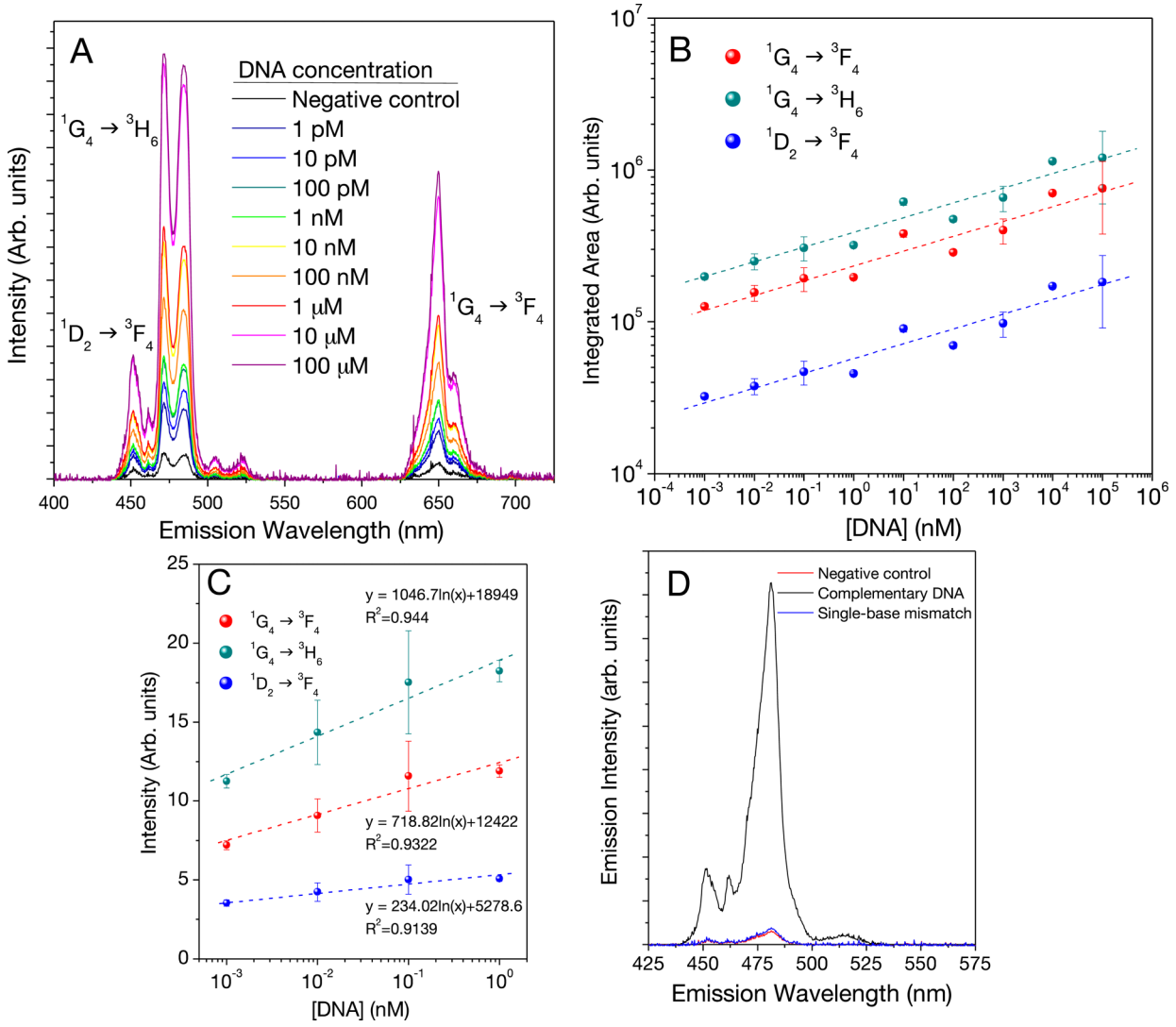

Figure 4. (A) Integrated area under the blue emission vs concentration of complementary DNA sequence. (B) Upconversion spectra in the blue region of the sensor upon adding different concentrations of target ssDNA sequence. (C) Linear dependence of emission intensity at the lower target DNA concentration levels. (D) Comparison of luminescent emission intensities of complementary, negative control, and single base mismatch DNA sequences.

upconversion, instead of directly quenching the blue emission. This indicates the sensitivity of the biosensor, i.e., the difference in intensity for two different concentrations ($\Delta I/\Delta$[DNA]), will be higher at lower concentrations.

Thus, in that range where the signal is normally weaker, even for small target DNA changes, the difference in luminescence intensity will be considerably high. Initial optical measurements showed nonlinear behavior for the higher target DNA concentrations. This may be attributed to the precipitation of the nanohybrids upon hybridization with the target DNA (Figure S6). At higher concentrations, DNA hybridization leads to induced aggregation, which resulted in the precipitation. This affected the linear dependence of the optical measurements. However, for lower concentrations ranging from 1 nM to 1 pM the emission intensity showed a sharp linear dependence, which lies well within the error (Figure 4C). This confirmed the higher sensitivity and reproducibility of our biosensor especially at the lowest target DNA concentration level down to 1 pM.

4. CONCLUSION

In conclusion, we have developed a new LRET-based DNA sensor that uses ssDNA functionalized PSA/SiO_2/UCNPs nanohybrids as the energy donor and water-soluble [$(ppy)_2$Ir-(dcbpy)$(4\text{-ABT})_2$]-AuNP conjugates as efficient quenchers, and its efficiency has been demonstrated down to the picomolar level. Since our LRET sensor is based on the use of UCNPs, the signal contrast has been excellent and offers other advantages such as the absence of autofluorescence and light scattering, making it an ideal optical biosensor. Also, the broad separation between the excitation wavelength and acceptor absorption, as well as between acceptor emissions and donor absorptions, eliminates the mixed signals or spectral cross-talk. The efficiency of Tm^{3+}, Yb^{3+} codoped UCNPs as donors has been demonstrated, and opens the door for the possibility of making multichannel sensors in combination with other lanthanides, like the most commonly used Er^{3+} ions.

In addition, the use of PSA nanoparticles that can be easily functionalized with different donor particles is an advantage in that regard. In addition, the high fluorescence quenching

DOI: 10.1021/acsami.5b02986
ACS Appl. Mater. Interfaces 2015, 7, 18257−18265

efficiency of $[(ppy)_2Ir(dcbpy)(4\text{-}ABT)_2]$/AuNP conjugates on PSA/SiO_2/UCNPs was also shown as the fluorescence is quenched from the root of the upconversion process instead of directly absorbing the emitted light from the UCNPs. Therefore, our results confirmed that PSA/SiO_2/UCNP// $[(ppy)_2Ir(dcbpy)(4\text{-}ABT)_2]$/AuNP conjugates could be an effective tool in a LRET-based assay and could be successfully applied in the development of more efficient optical sensors for the detection of various biomolecules. Our results have also provided a LRET system that is sensitive and simple to use in biological analyses. Further studies may pave the way to extend the applications of this new detection scheme in ultrasensitive multiplexed detection of wide range of biomolecular analytes.

■ ASSOCIATED CONTENT

Supporting Information

UV−vis absorption, PL emission spectra of the Ir(III) (Figure S1), representative TEM, XRD of the as synthesized $NaYF_4$:Tm^{3+}, Yb^{3+} nanoparticles, energy dispersive X-ray spectrum (EDX) and the XPS of $NaYF_4$:Tm^{3+}, Yb^{3+} decorated PSA/SiO_2 nanoparticles (Figure S3), TEM of gold nanoparticles (Figure S4) included. Optical images of $NaYF_4$:Tm^{3+},Yb^{3+} in hexane, citrate stabilized $NaYF_4$:Tm^{3+},Yb^{3+} in water, $NaYF_4$:Tm^{3+},Yb^{3+} tagged PSA/SiO_2 nanoparticles luminescence at 975 nm excitation (Figure S5). Schemes S1−S3 show complete synthesis of nanohybrids and DNA attachment. The Supporting Information is available free of charge on the ACS Publications website at DOI: 10.1021/acsami.5b02986.

■ AUTHOR INFORMATION

Corresponding Authors

*E-mail: vetrone@emt.inrs.ca.

*E-mail: m.zourob@qub.ac.uk or mzourob@alfaisal.edu.

Notes

The authors declare no competing financial interest.

■ ACKNOWLEDGMENTS

Authors are grateful for financial support from the Natural Sciences and Engineering Research Council (NSERC) of Canada as well as the Fonds de Recherche du Québec − Nature et Technologies (FRQNT) for supporting the research.

■ REFERENCES

(1) Jaiswal, J. K.; Mattoussi, H.; Mauro, J. M.; Simon, S. M. Long-Term Multiple Color Imaging of Live Cells Using Quantum Dot Bioconjugates. *Nat. Biotechnol.* **2002**, *21*, 47−51.

(2) Medintz, I. L.; Clapp, A. R.; Mattoussi, H.; Goldman, E. R.; Fisher, B.; Mauro, J. M. Self-Assembled Nanoscale Biosensors Based on Quantum Dot FRET Donors. *Nat. Mater.* **2003**, *2*, 630−638.

(3) Maestro, L. M.; Martín Rodríguez, E.; Vetrone, F.; Naccache, R.; Loro Ramírez, H.; Jaque, D.; Capobianco, J. A.; García Solé, J. Nanoparticles for Highly Efficient Multiphoton Fluorescence Bioimaging. *Opt. Express* **2010**, *23*, 23544−23553.

(4) Ju, Q.; Luo, W. Q.; Liu, Y. S.; Zhu, H. M.; Li, R. F.; Chen, X. Y. Poly(acrylic acid)-Capped Lanthanide-Doped BaFCl Nanocrystals: Synthesis and Optical Properties. *Nanoscale* **2010**, *2*, 1208−1212.

(5) Wang, F.; Wang, J.; Liu, X. Direct Evidence of a Surface Quenching Effect on Size-Dependent Luminescence of Upconversion Nanoparticles. *Angew. Chem.* **2010**, *122*, 7618−7622.

(6) Wang, F.; Liu, X. Recent Advances in the Chemistry of Lanthanide-Doped Upconversion Nanocrystals. *Chem. Soc. Rev.* **2009**, *38*, 976−989.

(7) Louis, U.; Bazzi, R.; Marquette, C. A.; Bridot, J. L.; Roux, S.; Ledoux, G.; Mercier, B.; Blum, L.; Perriat, P.; Tillement, O. Nanosized Hybrid Particles with Double Luminescence for Biological Labeling. *Chem. Mater.* **2005**, *17*, 1673−1682.

(8) Wang, L. Y.; Yan, R. X.; Huo, Z. Y.; Wang, L.; Zeng, J. H.; Bao, J.; Wang, X.; Peng, Q.; Li, Y. D. Fluorescence Resonant Energy Transfer Biosensor Based on Upconversion-Luminescent Nanoparticles. *Angew. Chem., Int. Ed.* **2005**, *44*, 6054−6057.

(9) Zhang, P.; Rogelj, S.; Nguyen, K.; Wheeler, D. Design of a Highly Sensitive and Specific Nucleotide Sensor Based on Photon Upconverting Particles. *J. Am. Chem. Soc.* **2006**, *128*, 12410−12411.

(10) Chen, Z. G.; Chen, H. L.; Hu, H.; Yu, M. X.; Li, F. Y.; Zhang, Q.; Zhou, Z. G.; Yi, T.; Huang, C. H. Versatile Synthesis Strategy for Carboxylic Acid−Functionalized Upconverting Nanophosphors as Biological Labels. *J. Am. Chem. Soc.* **2008**, *130*, 3023−3029.

(11) Peng, J. H.; Wang, Y. H.; Wang, J. L.; Zhou, X.; Liu, Z. H. A New Biosensor for Glucose Determination in Serum Based on Up-Converting Fluorescence Resonance Energy Transfer. *Biosens. Bioelectron.* **2011**, *28*, 414−420.

(12) Wang, Y. H.; Bao, L.; Liu, Z. H.; Pang, D. W. Aptamer Biosensor Based on Fluorescence Resonance Energy Transfer from Upconverting Phosphors to Carbon Nanoparticles for Thrombin Detection in Human Plasma. *Anal. Chem.* **2011**, *83*, 8130−8137.

(13) Yuan, Y. X.; Liu, Z. H. An Effective Approach to Enhanced Energy-Transfer Efficiency From Up-Converting Phosphors and Increased Assay Sensitivity. *Chem. Commun.* **2012**, *48*, 7510−7512.

(14) Wang, M.; Hou, W.; Mi, C. C.; Wang, W. X.; Xu, Z. R.; Teng, H. H.; Mao, C. B.; Xu, S. K. Immunoassay of Goat Antihuman Immunoglobulin G Antibody Based on Luminescence Resonance Energy Transfer between Near-Infrared Responsive $NaYF_4$:Yb, Er Upconversion Fluorescent Nanoparticles and Gold Nanoparticles. *Anal. Chem.* **2009**, *81*, 8783−8789.

(15) Chen, S. J.; Chang, H. T. Nile Red-Adsorbed Gold Nanoparticles for Selective Determination of Thiols Based on Energy Transfer and Aggregation. *Anal. Chem.* **2004**, *76*, 3727−3734.

(16) Wargnier, R.; Baranov, A. V.; Maslov, V. G.; Stsiapura, V.; Artemyev, M.; Pluot, M.; Sukhanova, A.; Nabiev, I. Energy Transfer in Aqueous Solutions of Oppositely Charged CdSe/ZnS Core/Shell Quantum Dots and in Quantum Dot−Nanogold Assemblies. *Nano Lett.* **2004**, *4*, 451−457.

(17) Fan, C. H.; Wang, S.; Hong, J. W.; Bazan, G. C.; Plaxco, K. W.; Heeger, A. J. Beyond Superquenching: Hyper-Efficient Energy Transfer From Conjugated Polymers to Gold Nanoparticles. *Proc. Natl. Acad. Sci. U. S. A.* **2003**, *100*, 6297−6301.

(18) Dubertret, B.; Calame, M.; Libchaber, A. J. Single-Mismatch Detection Using Gold-Quenched Fluorescent Oligonucleotides. *Nat. Biotechnol.* **2001**, *19*, 365−370.

(19) Maxwell, D. J.; Taylor, J. R.; Nie, S. Self-Assembled Nanoparticle Probes for Recognition and Detection of Biomolecules. *J. Am. Chem. Soc.* **2002**, *124*, 9606−9612.

(20) Ye, W. W.; Tsang, M. K.; Liu, X.; Yang, M.; Hao, J. Upconversion Luminescence Resonance Energy Transfer (LRET)-Based Biosensor for Rapid and Ultrasensitive Detection of Avian Influenza Virus H7 Subtype. *Small* **2014**, *10*, 2390−2397.

(21) Li, M. J.; Jiao, P. C.; Lin, M.; He, W. W.; Chen, G. N.; Chen, X. High Electrochemiluminescence of a New Water-Soluble Iridium (III) Complex for Determination of Antibiotics. *Analyst* **2011**, *136*, 205−210.

(22) Shiu, H. Y.; Wong, M. K.; Che, C. M. Turn-on FRET-Based Luminescent Iridium (III) Probes for the Detection of Cysteine and Homocysteine. *Chem. Commun.* **2011**, *47*, 4367−4369.

(23) Li, C. X.; Lin, J.; Guo, Y. S.; Zhang, S. S. A Novel Electrochemiluminescent Reagent of Cyclometalated Iridium Complex-Based DNA Biosensor and its Application in Cancer Cell Detection. *Chem. Commun.* **2011**, *47*, 4442−4444.

(24) Bandini, M.; Bianchi, M.; Valenti, G.; Piccinelli, F.; Paolucci, F.; Monari, M.; Umani-Ronchi, A.; Marcaccio, M. Electrochemiluminescent Functionalizable Cyclometalated Thiophene-Based Iridium(III) Complexes. *Inorg. Chem.* **2010**, *49*, 1439−1448.

DOI: 10.1021/acsami.5b02986
ACS Appl. Mater. Interfaces 2015, 7, 18257−18265

(25) Boyer, J. C.; Vetrone, F.; Cuccia, L. A.; Capobianco, J. A. Synthesis of Colloidal Upconverting $NaYF_4$ Nanocrystals Doped with Er^{3+}, Yb^{3+} and Tm^{3+}, Yb^{3+} via Thermal Decomposition of Lanthanide Trifluoroacetate Precursors. *J. Am. Chem. Soc.* **2006**, *128*, 7444−7445.
(26) Simpson, D. A.; Gibbs, W. E.; Collins, S.; Blanc, W.; Dussardier, B.; Monnom, G.; Peterka, P.; Baxter, G. W. Visible and Near Infra-Red Up-Conversion in Tm^{3+}/Yb^{3+} Co-Doped Silica Fibers Under 980 nm Excitation. *Opt. Express* **2008**, *16*, 13781−13799.
(27) Shi, W.; Sahoo, Y.; Swihart, M. T. Gold Nanoparticles Surface-Terminated With Bifunctional Ligands. *Colloids Surf., A* **2004**, *246*, 109−113.

DOI: 10.1021/acsami.5b02986
ACS Appl. Mater. Interfaces 2015, 7, 18257−18265